Available online at www.sciencedirect.com

ScienceDirect

Ceramics International 39 (2013) 8633–8640

CERAMICS INTERNATIONAL

www.elsevier.com/locate/ceramint

Hydrothermal synthesis and visible-light photocatalytic activity of α-Fe_2O_3/TiO_2 composite hollow microspheres

Hua Tang[a,*], Du Zhang[a], Guogang Tang[a,b], Xiaorui Ji[a], Wenjing Li[a], Changsheng Li[a], Xiaofei Yang[a,*]

[a]*School of Materials Science and Engineering, Jiangsu University; Key Laboratory of high-end structural materials of Jiangsu Province Zhenjiang, Jiangsu 212013, PR China*

[b]*Department of Chemical Engineering, Zhenjiang College, Zhenjiang, Jiangsu 212003, PR China*

Received 26 January 2013; received in revised form 11 April 2013; accepted 11 April 2013
Available online 24 April 2013

Abstract

Novel α-Fe_2O_3/TiO_2 composite hollow spheres were successfully synthesized by a template-assisted precipitation reaction using urea as a precipitating agent and carbon spheres as templates in a mixed solvent of water and ethanol, and then calcined at 400 °C for 4 h. The as-prepared samples were characterized by X-ray diffraction, scanning electron microscopy, transmission electron microscopy, nitrogen adsorption–desorption isotherms, and vibrating sample magnetometer. The influence of calcination temperature and the molar ratio of titanium to iron (*R*) on the photocatalytic activity of the samples was investigated. The results indicated that the composite spheres show magnetic characteristics at room temperature and good photocatalytic activity under visible-light irradiation compare to the single-component α-Fe_2O_3 particles. This method can be further applied to synthesize nanocomposites of magnetic metal oxide and other metal oxide.

Keywords: D. TiO_2; Fe_2O_3; Composite hollow microspheres; Template-assisted hydrothermal synthesis; Photocatalytic activity

1. Introduction

In recent years, micrometer- and nanometer-sized hollow structures have attracted a great deal of attention because of their low density, high surface area, good surface permeability and large light-harvesting efficiencies [1–4]. Moreover, these materials can be widely applied in photoelectric devices, catalysis, drug delivery, chromatography separation, and chemical reactors [5–9]. Various synthetic methods were explored to prepare hollow nanomaterials including Ionic liquids (ILs), self-assembly techniques, hydrothermal techniques, template-assisted techniques, and chemically induced self-transformation [10–12]. Up to now, template-assisted synthetic method has proved to be the most-applied and most effective route to fabricate inorganic hollow structures.

Titanium dioxide (TiO_2), as one of the most important transition-metal functional oxides, has attracted extensive attention during the past decades for its superior physical and chemical properties and a wide variety of potential use in diverse fields such as solar energy conversion, environmental purification, and water treatment [13–16]. In particular, TiO_2 hollow naomaterials and nanocomposites have received more and more attention owing to their high photocatalytic activity, chemical stability, low cost and nontoxicity [17,18]. However, because of its wide band-gap energy (3.02 eV), TiO_2 can only harvest the spectrum with wave lengths in the near-ultraviolet (UV) region shorter than 387 nm, which accounts for merely 4–5% of the solar spectrum. Moreover, TiO_2 follows a relatively high electron–hole recombination rate, which is detrimental to its photoactivity. To solve this issue, different approaches such as transition metal doping, inorganic dye-sensitizing, valuable metal deposition and coupling titania with other semiconductors have been devoted to enhancing the photocatalytic activity of TiO_2 in which the response of the semiconductor was extended toward the visible region [19–21]. Up to now, it is still a great

*Corresponding author. Tel./fax: +86 511 8879 0268.
E-mail addresses: hutang79@yahoo.com.cn (H. Tang), xyang@ujs.edu.cn (X. Yang).

0272-8842/$ - see front matter © 2013 Elsevier Ltd and Techna Group S.r.l. All rights reserved.
http://dx.doi.org/10.1016/j.ceramint.2013.04.040

challenge to effectively immobilize or separate the TiO_2 particles in the photocatalytic system. Magnetic separation provides a very convenient approach for removing and recycling magnetic particles/composites by applying an appropriate magnetic field [22,23]. Compared to conventional nanopowder photocatalysts, TiO_2 magnetic composites such as Fe_2O_3–TiO_2 or Fe_3O_4–TiO_2 can be regarded as a promising photocatalyst for the environmental purification at the industrial scale as they can be more readily separated from the slurry system by the magnetic separation after photocatalytic reaction and recycled. Very recently, Yu et al. [24] fabricate a hierarchical porous γ-Fe2O3@SiO2@TiO2 composite photocatalyst with superior photocatalytic properties by an effective three-step approach. Mou et al. [25] developed an asymmetric shrinkage approach for the fabrication of magnetic γ-Fe_2O_3/TiO_2 Janus hollow bowls (JHBs) by constructing a precursor solution pair during the solvents evaporation process. Moreover the as-obtained products show an efficient visible-light photocatalytic activity and convenient magnetic separation for water purification.

Herein, novel α-Fe_2O_3/TiO_2 composite hollow spheres are successfully fabricated using carbon spheres prepared from saccharide solution as templates, and their visible-light photocatalytic activity and environment application are carefully investigated. In addition, we also investigated the effects of the molar ratio of iron to titanium (R) on the microstructures and properties, especially on the photocatalytic property.

2. Experimental

2.1. Synthesis of carbon spheres

All the reagents used in the experiments were in analytical grade (purchased from SCRC Chemical Co., China) and used without further purification. Carbon spheres were synthesized by the hydrothermal approach as reported previously [26]. In a typical synthesis, 6.0 g glucose was dissolved in 60 mL of distilled water under constant stirring. Then the aqueous solution was transferred to a 100 mL Teflon-lined stainless steel autoclave, maintained at 180 °C for 4 h. The black or puce precipitates were washed with distilled water and ethanol three times and dried at 60 °C for 8 h. In general, a longer hydrothermal reaction time results in the formation of larger carbonaceous polysaccharide spheres.

2.2. Synthesis of α-Fe_2O_3/TiO_2 hollow structures

The α-Fe_2O_3/TiO_2 hollow structures were prepared as follows: 1.8 g $CO(NH_2)_2$ and 0.3 g carbon spheres were dissolved in 54 mL ethanol/water mixed solvents with given volume ratio (Ve/Vw = 48 mL/6 mL). After vigorously magnetic stirring for 30 min by using a magnetic stirrer, a certain amount of $FeCl_3$ and tetrabutyl titanate (TBOT) was added into the above solution under vigorously stirring for another 10 min. The molar ratio of titanium to iron (R) varied from 2:1 to 2:3 (2:1, 2:1.5, 2:2, and 2:3). The mixture was then transferred into a 100 ml Teflon-lined stainless steel autoclave and sealed, and the autoclave was placed in a pre-heated oven at 60 °C for 48 h and naturally cooled down to room temperature. The α-Fe_2O_3/TiO_2 precursor thus obtained was collected by centrifugation, washed with distilled water and dried under vacuum at 60 °C for 10 h. Finally, the prepared sample was heated in an air atmosphere to a certain temperature (400 °C) and held at this temperature for 4 h to remove the carbon spheres template.

2.3. Characterization

The X-ray diffraction patterns were recorded using a D8 advance (Bruker-AXS) diffractometer with Cu Kα radiation ($\lambda = 0.1546$ nm). The morphologies and structures of the samples were characterized by scanning electron microscopy (SEM, JEOL JXA-840A) and transmission electron microscopy (TEM) with a Japan JEM-100CX II transmission electron microscopy. The Brunauer–Emmett–Teller (BET) surface area (S_{BET}) of the powders was analyzed by nitrogen adsorption in an ASAP2020 surface area and porosity analyzer (Micromeritics, USA). All the samples were degassed at 180 °C prior to nitrogen adsorption measurements. The BET surface area was determined by a multipoint BET method using the adsorption data in the relative pressure (P/P_0) range of 0.05–0.25. Desorption isotherm was used to determine the pore size distribution via the Barret–Joyner–Halender (BJH) method with cylindrical pore size [27]. The nitrogen adsorption volume at the relative pressure (P/P_0) of 0.994 was used to determine the pore volume and average pore sizes. Magnetic properties of the samples were measured by a model 4HF vibrating sample magnetometer (VSM, ADE Co. Ltd., USA).

2.4. Photocatalytic activity test

The evaluation of photocatalytic activity of the prepared samples for the photocatalytic decolorization of RhB aqueous solution was performed at ambient temperature. A 300 W halogen–tungsten through a UV-cutoff filter (>400 nm, 13.0 ± 0.5 mW cm^2 at 420 nm), which was positioned 10 cm away from the reactor, was used as a visible light source to trigger the photocatalytic reaction. Experiments were as follows: 0.05 g of the prepared α-Fe_2O_3/TiO_2 powder was dispersed in a 20 mL of RhB aqueous solution with a concentration of 1×10^{-5} M in a reaction cell. Before illumination, the suspensions were magnetically stirred in the dark for 60 min to ensure the establishment of an adsorption–desorption equilibrium between the photocatalyst powders and RhB. At given time intervals, 3 mL aliquots were sampled and centrifuged to remove photocatalyst powders. The filtrates were analyzed by recording the variations of the absorption-band maximum (553 nm) of RhB in the UV–vis spectrum. Total organic carbon of the solution was analyzed with the Apollo9000 TOC analyzer.

3. Results and discussion

Fig. 1 shows XRD patterns of the α-Fe_2O_3/TiO_2 samples prepared at R = 2:1.5 at 60 °C for 48 h and calcined at 400 °C

for 4 h. The major diffraction peaks are consistent with either those of the JCPDS file No. 21-1272 or those of the JCPDS file No. 33-0664, indicating that the products mainly consist of the tetragonal rutile TiO_2 phase and the hexagonal α-Fe_2O_3 phase. In addition, some peaks (located at 18.0°, 25.5°, 32.5°) that do not match either of these phases are from the solid solution of iron titanium oxide phase (Fe_2TiO_5), which is probably due to the formation of a Fe-rich layer at the surface of TiO_2.

The size and morphology of the products were identified by SEM, TEM and HRTEM. Fig. 2a shows SEM image of the as-prepared C@α-Fe_2O_3/TiO_2 composite nanostructures with diameters ranging from 0.5 μm to 1 μm obtained via the hydrothermal process before calcination. As shown Fig. 2b, it can be clearly seen that diameters of α-Fe_2O_3/TiO_2 hollow spheres decrease drastically and are about 600 nm in size after calcination. To get more information about the hollow structures, the samples were characterized by TEM. Fig. 2c is the typical TEM image of α-Fe_2O_3/TiO_2 hollow spheres, further confirming the hollow structure with a shell thickness of about 60 nm. It can be found that the shells of α-Fe_2O_3/TiO_2 hollow spheres are composed of randomly aggregated nanoparticles with sizes of about 15 nm. A HRTEM image reveals more details concerning the hybrid structure (Fig. 2d). The lattice fringe spacing of 0.37 nm and 0.35 nm are consistent with the interplanar distances of (012) plane of α-Fe_2O_3 and (110) plane of TiO_2.

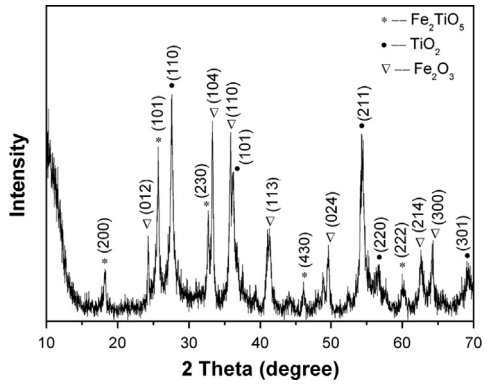

Fig. 1. XRD patterns of the products prepared at R=2:1.5 and calcined at 400 °C for 4 h.

To examine the surface area, as well as the pore size distribution, nitrogen adsorption/desorption analysis was conducted. As shown in Fig. 3a, the BET surface area of the as-prepared α-Fe_2O_3/TiO_2 hollow spheres is 31.8 m^2/g, which is higher than that of commercial iron oxide particles [28]. Fig. 3a shows the sample exhibits a type IV isotherm with a H3 hysteresis loop according to Brunauer–Deming–Deming–Teller (BDDT), indicating the presence of mesopores (2–50 nm). In addition, the observed hysteresis loops shifts to a high relative pressure $P/P_0 \approx 1$, suggesting the presence of large pores ($>$ 50 nm). The corresponding pore size distribution curve is shown in Fig. 3b. It can be seen that the α-Fe_2O_3/TiO_2 hollow spheres contained small mesopores (ca. 3 nm) and larger mesopores with a maximum pore diameter of ca. 26 nm. This result is consistent with the TEM observation (Fig. 2d). According to previous reports [27–29], the larger specific BET surface

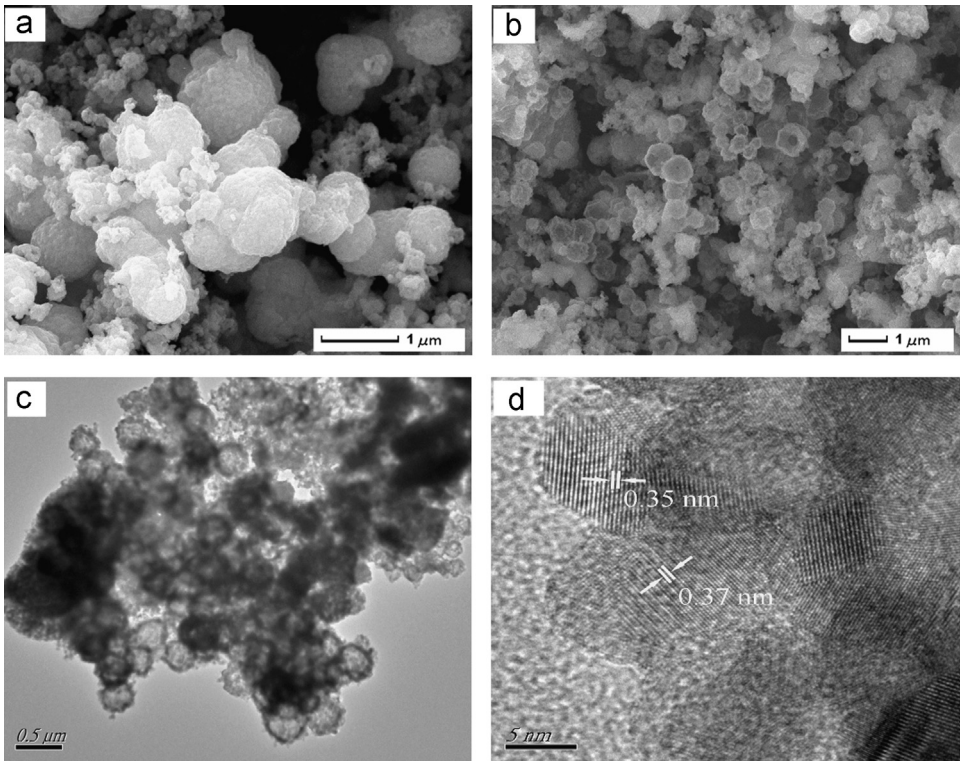

Fig. 2. SEM images of the α-Fe_2O_3/TiO_2 hollow spheres prepared at R=2:1.5 before calcination (a) and after calcination (b) at 400 °C for 4 h; (c, d) TEM and HR-TEM images of the α-Fe_2O_3/TiO_2 hollow structure after calcination.

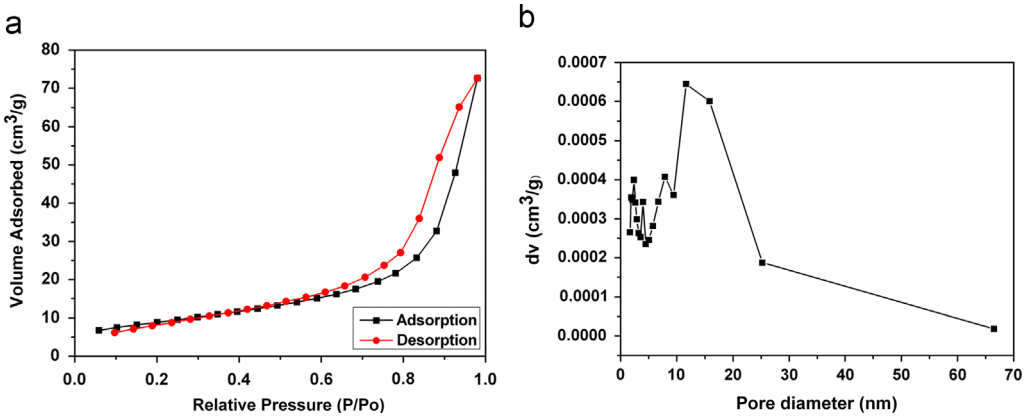

Fig. 3. Nitrogen adsorption–desorption isotherms (a) and pore-size distribution curve (b) for the as-obtained α-Fe_2O_3/TiO_2 hollow spheres.

area and mesoporous structure would be beneficial to adsorb the organic pollutants onto the surface of the photocatalyst.

Fig. 4 shows the UV-visible absorption spectra of the α-Fe_2O_3/TiO_2 hollow spheres. Pure TiO_2 only absorbed ultraviolet radiation of less than 400 nm (not shown here). The Fe_2O_3/TiO_2 composite hollow spheres samples exhibited not only stronger absorption in the ultraviolet region of less than 400 nm but also adequate and strong absorption in the visible light region of 400–700 nm. It indicates that Fe_2O_3/TiO_2 composite hollow spheres samples can also be used under visible light. In the present condition, Fe^{3+} was doped with the TiO_2 lattice, resulted in the reduction of the band gap. Additionally, the band gap of Fe_2O_3 was only 2.2 eV. The presence of this narrow band gap semiconductor, as well as the reduced TiO_2 band gap, greatly ameliorated the light absorption properties of the Fe_2O_3–TiO_2 composites, and enabled the absorption of visible light.

The photocatalytic activity of the samples was evaluated by monitoring the decoloration of RhB in aqueous solution. Prior to detailed evaluation of photocatalytic activities of the prepared samples, the concentration of RhB in the aqueous solution decreased slightly before illumination due to the adsorption in the dark. Most of the concentration decrease occurred during irradiation, and then the decrease in RhB concentration during irradiation was attributed to chemical reaction rather than adsorption. Additionally, it was also noticed that the degradation of RhB did not occur in the absence of catalysts under visible light under the experimental conditions. The low but not negligible activity can be attributed to a self-photosensitized process [29,29]. However, the efficiency is very low because of the fairly slow interfacial electron-transfer rate. For convenience, we assumed that the concentration of RhB after desorption–adsorption equilibrium was the initial concentration, C_0. Fig. 5a shows the temporal evolution of the absorption spectra of RhB under visible light irradiation in the presence of α-Fe_2O_3/TiO_2 hollow spheres. The absorption peak at 553 nm drops gradually with increasing irradiation time and almost disappears after 180 min, indicating that the α-Fe_2O_3/TiO_2 hollow spheres exhibits excellent photocatalytic activity during the reaction. Fig. 4b shows the effects of visible light irradiation time (t) on the normalized

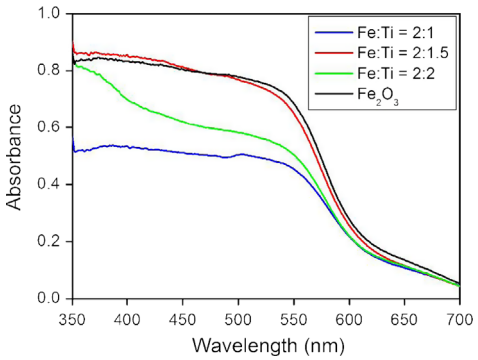

Fig. 4. UV–vis absorption spectrum of Fe_2O_3/TiO_2 composite hollow spheres.

RhB concentration (C_t/C_0) for the RhB aqueous solutions containing different catalysts. It can be seen that when RhB solution was irradiated in the absence of photocatalyst, a decoloration rate of less than 10% after 180 min was detected, which is considered to come from the photolysis of organic dye RhB. However, when P25, pure Fe_2O_3, α-Fe_2O_3/TiO_2 hollow spheres photocatalysts were employed, the decoloration rate of organic dye RhB after 180 min was about 50%, 75% and 98% respectively. To determine the mineralization degree of organic dye RhB, TOC analyses were performed on dispersions at different visible-light irradiation times. It can be clearly seen from TOC data (Fig. 5c) that TOC diminishes gradually as the exposure time increases and ca. 42% TOC removal is obtained at 360 min. It is then conclusive that the decoloration of RhB in the presence of photocatalyst is majorly attributed to the photocatalytic degradation of RhB along with slight photolysis of dye under visible light irradiation. Moreover, the α-Fe_2O_3/TiO_2 hollow spheres exhibit better visible-light photocatalytic activity than that of the α-Fe_2O_3 or pure TiO_2 sample. The enhanced visible-light photocatalytic activity can be attributed to the increase in specific surface area, the separation of photo-induced electron–hole pairs and hollow microarchitecture [30]. The magnetic properties of photocatalysts are favorable in the water treatment because it can be conveniently separated by magnetic separation technology [31]. Magnetic hysteresis measurement for α-Fe_2O_3/TiO_2 hollow spheres is carried out in applied magnetic field at

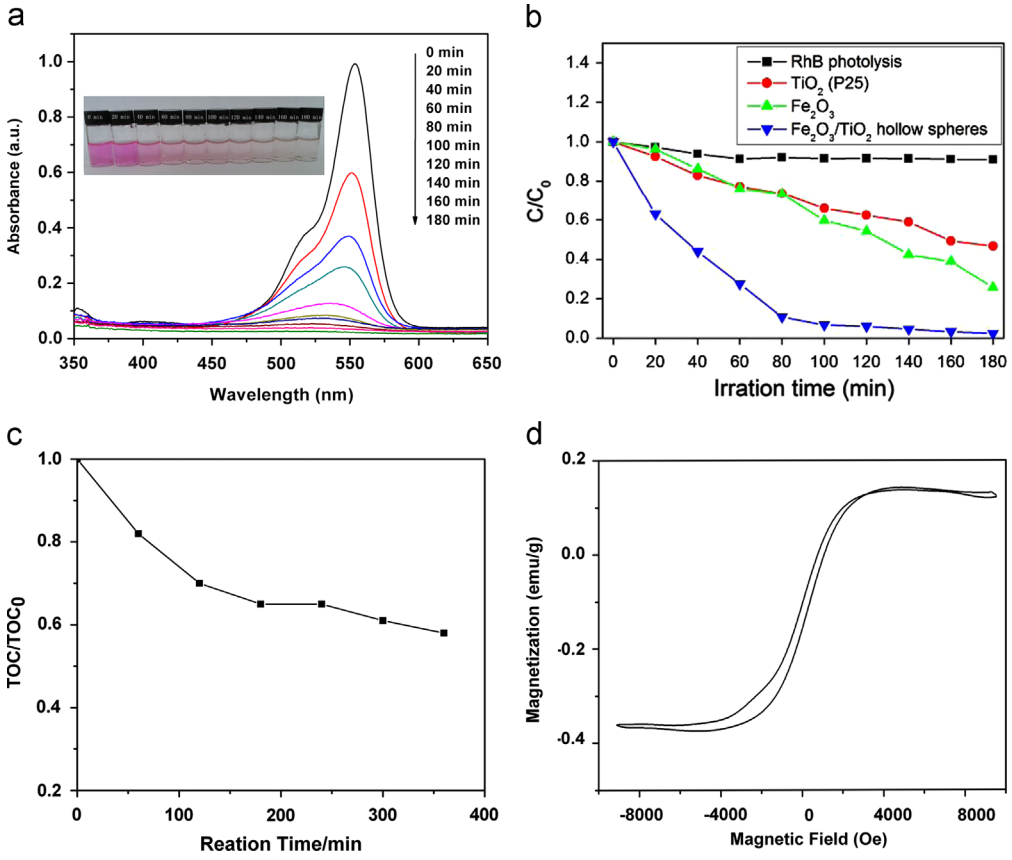

Fig. 5. Absorption spectra of the RhB solution containing α-Fe_2O_3/TiO_2 hollow spheres after different irradiation times with visible light (a); normalized RhB concentration versus visible light irradiation time for the RhB aqueous solutions with the different catalysts (b); Changes in solution TOC during RhB degradation (c). Initial solution: 10 μmol L^{-1} RhB+25 μmol L^{-1} α-Fe_2O_3/TiO_2 hollow spheres; 200 W metal halide lamp, pH 7.0; and Magnetic hysteresis loops of α-Fe_2O_3/TiO_2 hollow spheres (d).

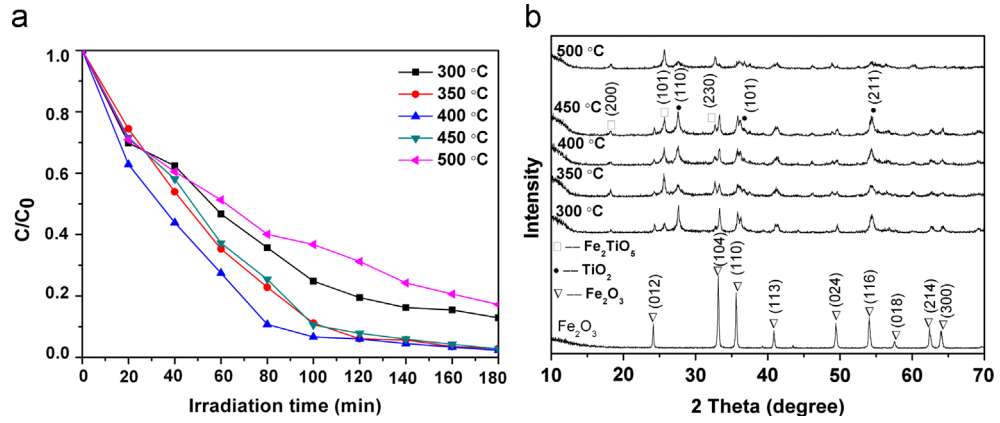

Fig. 6. Comparision of the photocatalytic activity of the samples after calcination at different temperature (300–500 °C) (a); XRD patterns of the products prepared after calcination at different temperature (300–500 °C) (b).

room temperature, with the field sweeping from −18 to 18 kOe. As shown Fig. 4c, the magnetization measurement result of the α-Fe_2O_3/TiO_2 hollow spheres is indicative of the presence of ferromagnetic components. The saturation magnetization (Ms) is 8.4 emu/g. In addition, from Fig. 4c it can be seen that no saturation of the magnetization as a function of the field is observed up to the maximum applied magnetic field.

To further study the photocatalytic activity of the α-Fe_2O_3/TiO_2 hollow spheres, the time dependence of the relative concentration of RhB for the samples calcined at different temperature (300–500 °C), is depicted in Fig. 6a. It was easily be found that the photocatalytic activity of the sample α-Fe_2O_3/TiO_2 hollow spheres increased gradually with the increasing calcination temperature up to 400 °C. With the

further increase of the temperature to 450 °C, the photocatalytic activity decreased slightly. When the calcinations temperature reached 500 °C, the sample has the lowest photocatalytic activity. Fig. 5b shows XRD patterns of the α-Fe_2O_3/TiO_2 samples calcined at different temperature for 4 h. The XRD results indicate that the sample calcined at 300 °C consists of both α-Fe_2O_3 and rutile TiO_2 along with a small amount of iron titanium oxide phase (Fe_2TiO_5). With the increase of calcination temperature (T), the intensities of diffraction peaks of Fe_2TiO_5 increased. However, When T reached 500 °C, the relative peak intensities of TiO_2 phase decreases obviously, indicated low photocatalytic activity. The improved photocatalytic activity of α-Fe_2O_3/TiO_2 samples calcined at 350–450 °C might be attributed to their good crystallinity, fewer defects and low recombination rate of the electron–hole pair due to the synergetic effect among the components of TiO_2, Fe_2TiO_5, Fe_2O_3 in the nanostructure.

In addition, it is found that the molar ratio of iron to titanium (R=n(Fe)/n(Ti)) plays a vital role on the photocatalytic activity of the final products. The XRD patterns of α-Fe_2O_3/TiO_2 obtained at different R calcined at 400 °C are shown in Fig. 7a. At R=2:1, the sample consists of α-Fe_2O_3 and rutile phase. When R increased to 2:1.5 and 2:2, the peaks located at 2 theta values of 18.09°, 25.55° and 32.51° suggested the appearance of a Fe_2TiO_5 phase (JCPDS No. 41-1432), which was mixed with α-Fe_2O_3 and rutile phase. However, further increase R to 2:3, the sample is composed of α-Fe_2O_3 and rutile phase, and no Fe_2TiO_5 phase was observed. Fig. 7b–d show TEM images of as-prepared α-Fe_2O_3/TiO_2 obtained at various R. Fig. 6c–d clearly reveal the structure of α-Fe_2O_3/

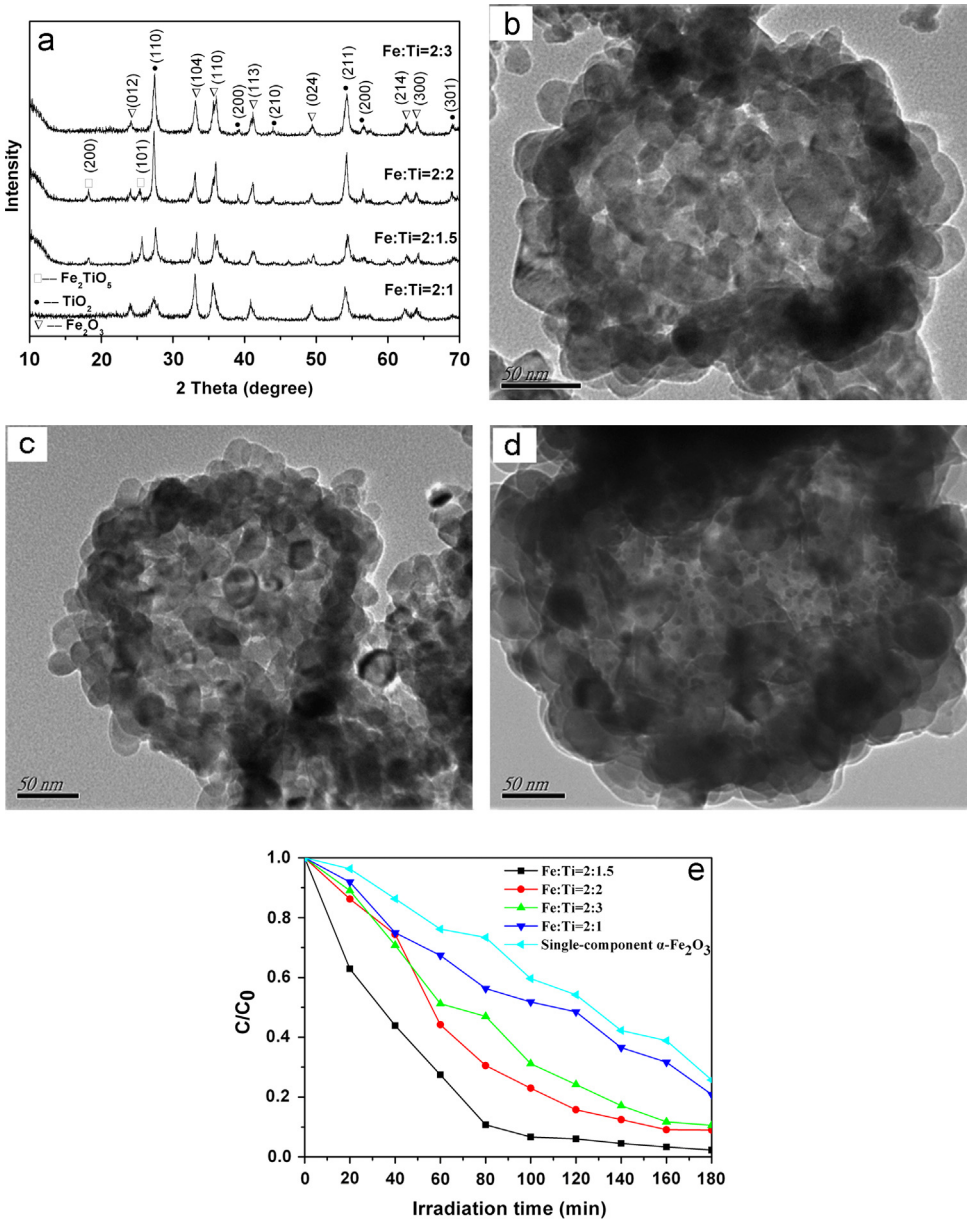

Fig. 7. XRD patterns (a) of the products prepared with varying R calcined at 400 °C for 4 h; TEM images of the products prepared with varying R: (b) 2:1, (c) 2:2, (d) 2:3, and comparison of the photocatalytic activity of the samples with varying R (e).

TiO_2 composite hollow spheres was composed of randomly aggregated nano-particles with sizes of about 18 nm. Moreover, the doped TiO_2 could hinder slightly the increase of the composite nanoparticles size.

The photocatalytic activity of the samples with varying R was evaluated by monitoring the degradation of RhB in aqueous solution. R exhibited obvious influence on the photocatalytic activity of α-Fe_2O_3/TiO_2 composite hollow spheres (Fig. 7e). Compared with pure α-Fe_2O_3, the α-Fe_2O_3/TiO_2 composite hollow spheres with different mass ratios all exhibit better photocatalytic activity. In particular, the photocatalytic activity of the samples obtained at R=2:1.5 reaches a maximum value. The high photocatalytic activity might be partially due to its more intense absorption in the visible light range (Fig. 4), more red shift in the band gap transition, and larger surface compared with other Fe_2O_3/TiO_2 composites, which resulted in more photogenerated electrons and holes participating in the photocatalytic reactions under visible light and more pollutants adsorbed on the surface of the photo catalyst.

4. Conclusions

In summary, α-Fe_2O_3/TiO_2 composite hollow spheres were successfully synthesized on a large scale by a controlled template-assisted hydrothermal precipitation reaction. The results indicated that the composite spheres show a high photocatalytic activity on the degradation of an RhB solution. Calcination temperature and the molar ratio of titanium to iron (R) should play important roles on photocatalytic activity of the samples. Moreover, the prepared samples can be more readily separated and reused from the slurry system by the magnetic separation after photocatalytic reaction compared to conventional photocatalysts. In addition, this work also provided a simple and general method for fabricating nanocomposites of magnetic metal oxide and other metal oxide, which may find wider applications involve drug delivery, microcontainers, microreactors, sensors, and so forth.

Acknowledgments

This work was financially supported by the National Natural Science Foundation of China (51275213 and 51102116), the Jiangsu National Nature Science Foundation (BK2011534 and BK2011480), a Project Funded by the Priority Academic Program Development of Jiangsu Higher Education Institutions, and the Open Project of Key Laboratory of Tribology of Jiangsu Province (Kjsmcx2011002 and Kjsmcx1005).

References

[1] K. An, S.G. Kwon, M. Park, et al., Synthesis of uniform hollow oxide nanoparticles through nanoscale acid etching, Nano Letters 8 (2008) 4252–4258.

[2] H.L. Zhou, Z. Zou, S. Wu, et al., Rapid synthesis of TiO_2 hollow nanostructures with crystallized walls by using CuO as template and microwave heating, Material Letters 65 (2011) 1034–1036.

[3] J.G. Yu, S.W. Liu, H.G. Yu, Microstructures and photoactivity of mesoporous anatase hollow microspheres fabricated by fluoride-mediated self-transformation, Journal of Catalysis 249 (2007) 59–66.

[4] S.Z.,J.Y. Yang, Y. Liu, et al., Mesoporous Fe_2O_3-doped TiO_2 nanostructured fibers with higher photocatalytic activity, Journal of Colloid and Interface Science 355 (2011) 328–333.

[5] Q.H. He, Z.X. Zhang, J.X. Xiong, et al., A novel biomaterial—Fe_3O_4: TiO_2 core–shell nano-particles with magnetic performance and high visible light photocatalytic activity, Optical Materials, 31, 380–384.

[6] D.J. Du, M.H. Cao, Ligand-assisted hydrothermal synthesis of hollow Fe_2O_3 urchin-like microstructures and their magnetic properties, Journal of Physical Chemistry C 112 (2008) 10754–10758.

[7] R.S. Yuan, X.Z. Fu, X.C. Wang, et al., Template synthesis of hollow metal oxide fibers with hierarchical architecture, Chemistry of Materials 18 (2006) 4700–4705.

[8] S. Peng, S. Sun, Synthesis and characterization of hollow Fe_3O_4 nanoparticles, Angewandte Chemie International Edition 46 (2007) 4155–4158.

[9] J.G. Yu, H.T. Guo, S.A. Davis, et al., Fabrication of hollow inorganic microspheres by chemically induced self-transformation, Advanced Functional Materials 16 (2006) 2035–2041.

[10] Y.J. Xiong, Z.Q. Li, X.X. Li, et al., Thermally stable hematite hollow nanowires, Inorganic Chemistry 43 (2004) 6540–6542.

[11] X. Lu, F. Huang, J. Wu, et al., Intelligent hydrated-sulfate template assisted preparation of nanoporous TiO_2 spheres and their visible-light application, ACS Applied Materials Interaces 3 (2011) 566–572.

[12] J.G. Yu, X.X. Yu, Hydrothermal synthesis and photocatalytic activity of zinc oxide hollow spheres, Environmental Science Technology 42 (2008) 4902–4907.

[13] X. Wang, B. Huang, Z. Wang, X. Qin, et al., Synthesis of anatase TiO_2 tubular structures microcrystallites with a high percentage of {001} facets by a simple one-step hydrothermal template process, Chemistry European Journal 1 (2010) 7106–7109.

[14] B. Liu, E.S. Aydil, Growth of oriented single-crystalline rutile TiO_2 nanorods on transparent conducting substrates for dye-sensitized solar cells, Journal of the American Chemical Society 131 (11) (2009) 3985–3990.

[15] Y. Dai, C.M. Cobley, J. Zeng, et al., Synthesis of anatase TiO_2 nanocrystals with exposed {001} facets, Nano Letters 9 (2009) 2455–2459.

[16] H. Lin, L. Li, M. Zhao, et al., Synthesis of high-quality brookite TiO_2 single-crystalline nanosheets with specific facets exposed: tuning catalysts from inert to highly reactive, Journal of the American Chemical Society 134 (20) (2012) 8328–8331.

[17] X. Zhang, Y. Sun, X. Cui, et al., Carbon-incorporated TiO_2 microspheres: facile flame assisted hydrolysis of tetrabutyl orthotitanate and photocatalytic hydrogen production, International Journal of Hydrogen Energy 37 (2012) 1356–1365.

[18] Q. Zhang, W. Li, S.X. Liu, Controlled fabrication of nanosized TiO_2 hollow sphere particles via acid catalytic hydrolysis/hydrothermal treatment, Powder Technology 212 (2011) 145–150.

[19] A. Aziz, K. Yong, S. Ibrahim, et al., Enhanced magnetic separation and photocatalytic activity of nitrogen doped titania photocatalyst supported on strontium ferrite, Journal of Hazardous Material 199–200 (2012) 143–150.

[20] J.M. Herrmann, Titania-based true heterogeneous photocatalysis, Environmental Science and Pollution Research 19 (2012) 3655–3665.

[21] J.M. Herrmann, Detrimental cationic doping of titania in photocatalysis: why chromium Cr^{3+}-doping is a catastrophe for photocatalysis both under UV– and visible irradiations, New Journal of Chemistry 36 (2012) 883–890.

[22] R.V. Mambrinia, T.L. Fonsecaa, A. Diasb, et al., Magnetic composites based on metallic nickel and molybdenum carbide: a potential material for pollutants removal, Journal of Hazardous Material 241–242 (2012) 73–81.

[23] T. Zhang, X.L. Yan, D.D. Sun, Hierarchically multifunctional K-OMS-2/TiO_2/Fe_3O_4 heterojunctions for the photocatalytic oxidation of humic acid under solar light irradiation, Journal of Hazardous Material 243 (2012) 302–310.

[24] X.X. Yu, S.W. Liu, J.G. Yu, Superparamagnetic γ-Fe_2O_3@SiO_2@TiO_2 composite microspheres with superior photocatalytic properties, Applied Catalysis B: Environmental 104 (2011) 12–20.

[25] F.Z. Mou, L.L. Xu, H.R. Ma, et al., Facile preparation of magnetic γ-Fe_2O_3@TiO_2 Janus hollow bowls with efficient visible-light photocatalytic activities by asymmetric shrinkage, Nanoscale 4 (2012) 4650–4657.

[26] J.G. Yu, X.X. Yu, B.B. Huang, et al., Hydrothermal synthesis and visible-light photocatalytic activity of novel cage-like ferric oxide hollow spheres, Crystal Growth and Design 9 (2009) 1474–1480.

[27] J.G. Yu, J.C. Yu, M.P. Leung, et al., Effects of acidic and basic hydrolysis catalysts on the photocataytic activity and microstructures of bimodal mesoporous titania, Journal of Catalysis 217 (2003) 69–78.

[28] Y.J. Li, X.M. Zhou, W. Chen, et al., Photodecolorization of Rhodamine B on tungsten-doped TiO_2/activated carbon under visible-light irradiation, Journal of Hazardous Material 227–228 (2012) 25–33.

[29] D. Nassoko, Y.F. Li, H. Wang, et al., Nitrogen-doped TiO_2 nanoparticles by using EDTA as nitrogen source and soft template: simple preparation, mesoporous structure, and photocatalytic activity under visible light, Journal of Alloys Compdunds 540 (2012) 228–235.

[30] J.G. Yu, Y. Su, B. Cheng, Template-free fabrication and enhanced photocatalytic activity of hierarchical macro-/mesoporous titania, Advanced Functional Materials 17 (2007) 1984–1990.

[31] J.G. Yu, X.X. Yu, B. Huang, et al., Hydrothermal synthesis and visible-light photocatalytic activity of novel cage-like ferric oxide hollow spheres, Crystal Growth and Design 9 (2009) 1474–1480.